

Response to Referee #2

The manuscript did a very comprehensive study covering a very complex sea-air interaction through the link: volcano eruption - atmospheric pressure waves - tsunamis - gravity waves - mesosphere airglow. This manuscript provides important and likely first observations of volcano-related Lamb and gravity waves in the mesosphere airglow. In general, the authors provide evidence and arguments to support their conclusions. But I think the provided evidence is a little weak, more like a correlation between two, not robust enough to prove the generation relation. The Tonga volcano and related tsunami/waves have been well observed and reported; there should be good cross-verification between this study and previous studies. It is fine that the presented results are different from those previous studies, but you need to provide explanations. As the manuscript mentioned, many presented results are the first ever observed, so more careful reasoning and analysis are needed to support the observations. Five waves (Lamb wave L0, L1, and three gravity waves) were observed and reported in this study; I have concerns about each of them.

Thank you very much for your thoughtful, professional, and constructive comments concerning our manuscript entitled “Upper Atmosphere Responses to the 2022 Hunga Tonga-Hunga Ha’apai Volcanic Eruption via Acoustic-Gravity Waves and Air-Sea Interaction”. Those comments are all valuable and very helpful for revising and improving our paper, as well as the important guiding significance to our researches. We have studied concerns carefully and have made corrections which we hope meet with approval. The detailed point-by-point responses are given below.

1. Lamb waves have a vertical phase front below the thermosphere or zero vertical wave numbers. This means what you observe in the mesosphere should look the same or very similar to what is observed in the stratosphere. Many studies have reported the Lamb wave in the brightness temperature or IR radiation from geostationary satellites such as GOES (<https://agupubs.onlinelibrary.wiley.com/doi/full/10.1029/2023GL106097>), Himawari-8 (<https://agupubs.onlinelibrary.wiley.com/doi/full/10.1029/2022GL098324>). So, I would expect that the wave pattern in the mesosphere OH airglow looks very similar to these studies, like a solitary wave with one strong leading wave with much weaker trailing waves. What you show in the OH airglow images are stable wave trains? You show the surface pressure for the L0/L1 mode; both seem to be like solitary waves. (You should show the time derivative of the pressure to emphasize the wave.) Are you able to get the Himawari-8 brightness temperature and compare it with your OH airglow results, then you will have the full link of surface-> stratosphere->mesosphere.

Response:

Thank you very much for your comment. This is a very good question.

Yes, you are right. Lamb waves have a vertical phase front below the thermosphere or zero vertical wave numbers in the vertical direction and like a solitary wave with one strong leading wave with much weaker trailing waves in the horizontal direction, especially more pronounced in the lower atmosphere.

It is seen from model simulations that the wave amplitudes of L0 and L1 modes are not uniform at the wave front. This non-uniformity becomes more pronounced in the upper atmosphere (e.g. Figure 2 of Liu et al., 2023), probably as a result of the large variation of the background atmosphere propagation conditions. It is thus possible that over certain regions the trailing waves become comparable with the leading wave.

In addition, due to the smaller field of view of the airglow imager compared to satellite observations, some structures may be related to local fine structures, especially in the middle and upper layers where many internal waves have significant amplitudes, which may be relatively more significant than Lamb waves (Lamb waves have smaller amplitudes than internal waves).

Based on your suggestion, we have incorporated the Himawari-8 brightness temperature data (Otsuka, 2022) into this study to form a more complete observation chain of surface->stratosphere->mesosphere (Figure 5).

From the Figure 5, it can be seen that the phase of the lamb wave is almost vertical from the ground to the stratosphere and then to the mesosphere.

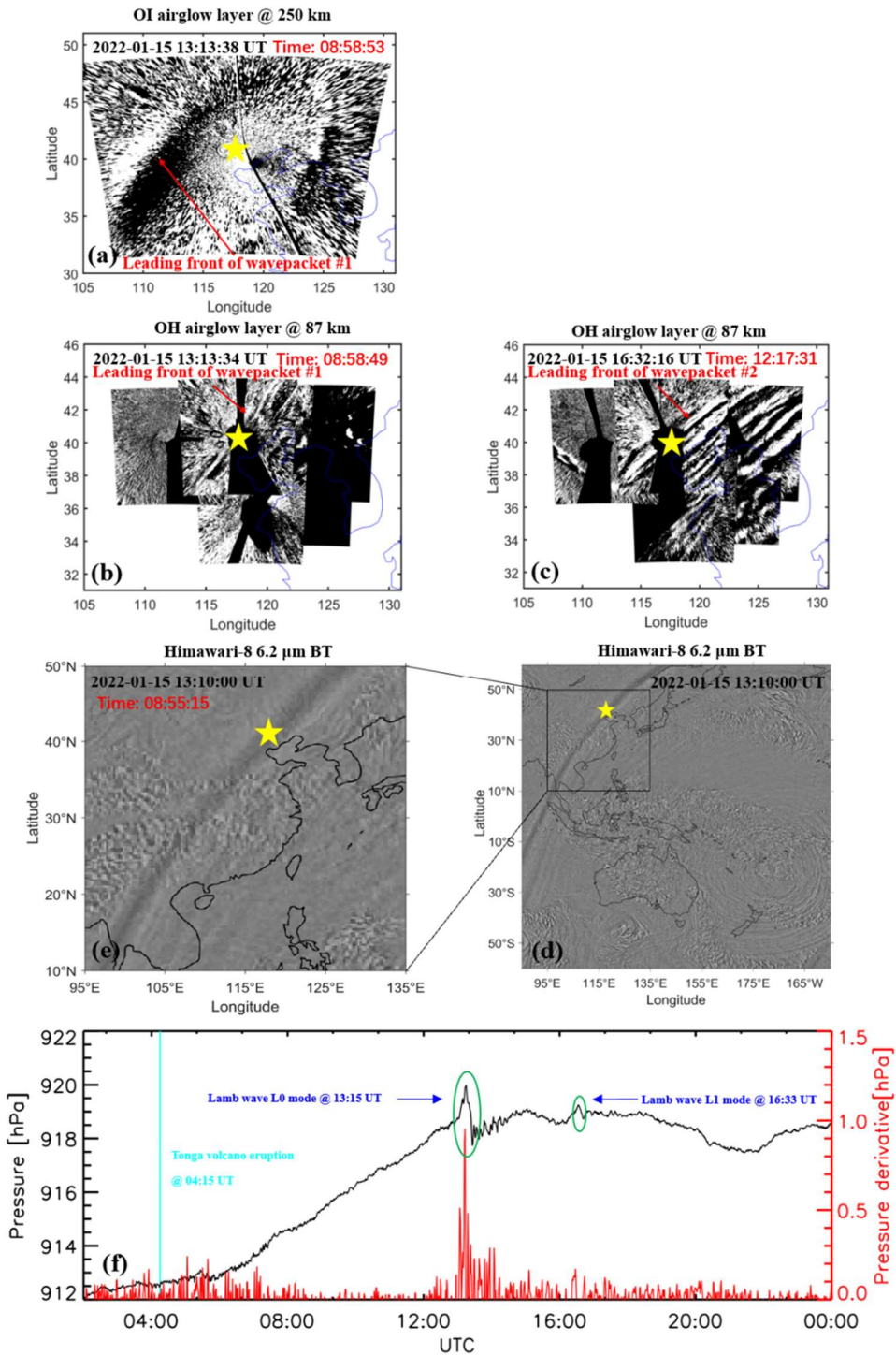


Figure 5 (a) OI 630 nm airglow observation at 13:13:18 UT. OH airglow network observations when (b) wave packet #1 and (c) wave packet #2 pass through the zenith direction of Xinglong Station at 13:13:34 UT and at 16:32:16 UT, respectively. (d)-(e) Himawari-8 6.2 μm brightness temperature at 13:10:00 UT. (f) The surface time series of surface pressure obtained from Xinglong observation station. The red line represents the time derivative of the pressure. The sudden change of air pressure at 13:15 UT indicates the arrival time of Lamb wave L0. A small disturbance of air pressure occurs at 16:33 UT indicates the arrival time of Lamb wave L1. The yellow stars represent the location of the Xinglong station.

References

- Liu, H.-L., Wang, W., Huba, J. D., Lauritzen, P. H., & Vitt, F. (2023). Atmospheric and ionospheric responses to Hunga-Tonga volcano eruption simulated by WACCM-X. *Geophysical Research Letters*, 50, e2023GL103682. <https://doi.org/10.1029/2023GL103682>
- Otsuka, S. (2022). Visualizing Lamb waves from a volcanic eruption using meteorological satellite Himawari-8. *Geophysical Research Letters*, 49, e2022GL098324. <https://doi.org/10.1029/2022GL098324>

2. Regarding the L0/L1 mode (wave #1 and #2), this manuscript seems to be one of the few that report the weaker L1 mode. You need a better estimate of the wave parameters including wavelength, period, and amplitude (airglow intensity fluctuations to be compared with L0), to justify the observations.

Response:

Thank you very much for your comment and suggestion.

Yes, you are right. The wave parameters need to be well estimated, and we use the cross spectral analysis method to estimate the wave parameters.

The detailed spectral analysis process is as follows

The airglow image was calibrated with the help of standard star map (Garcia et al., 1997) and projected into geospatial space. The background radiation is removed by differential method (Swenson and Mende,1994), to highlight atmospheric fluctuations. The atmospheric wave parameters (horizontal wavelength λ_h , observed speed c , and the relative intensity perturbation I'/I) are extracted from spectral analysis method. Figure 2c presents the two-dimensional cross spectrum obtained from Figures 2a and 2b. Zonal (k_x) and meridional (k_y) wave numbers are determined from the peak position of the spectra. The horizontal wavelengths λ_h are obtained from the expression of

$\lambda_h = 2\pi / \sqrt{k_x^2 + k_y^2}$. The observed speeds c are calculated from the phase (φ) (Figure 2d) at the maximum peak of the cross spectrum as $c = \frac{\varphi \lambda_h}{2\pi \Delta t}$, where Δt is the time

interval between the two TD images. The amplitudes of intensity perturbations were calculated by integrating the power surrounding the central peaks of the power spectrum. To eliminate noise, the energy of the wave spectrum should be greater than 10% of the total spectrum (Tang et al., 2005).

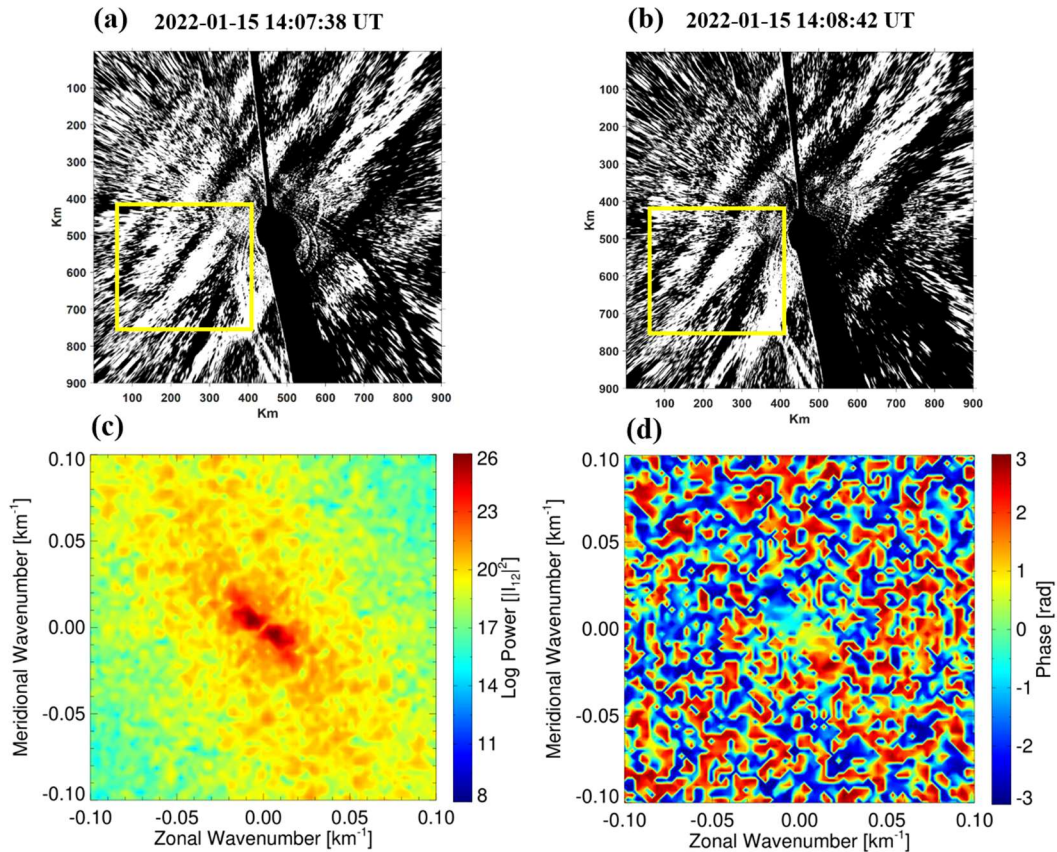


Figure 2 The time difference images (a-b) obtained from the Xinglong OH airglow imager on the night of 15 February 2022. Each image is projected on an area of 250 km × 250 km. The (c) cross spectrum and (d) phase of the time difference images from a and b using 2-D fast Fourier transform.

References

Garcia, F. J., Taylor, M. J., and Kelley, M. C.: Two-dimensional spectral analysis of mesospheric airglow image data, *Appl. Optics*, 36 (29), 7374–7385, 1997.

Swenson, G. R. and Mende, S. B.: OH emission and gravity waves (including a breaking wave) in all-sky imagery from Bear Lake, UT, *Geophys. Res. Lett.*, 21, 2239–2242, 1994.

Tang, J., Kamalabadi, F., Franke, S. J., Liu, A. Z., and Swenson, G. R.: Estimation of gravity wave momentum flux with spectroscopic imaging, *IEEE T. Geosci. Remote*, 43, 103–109, 2005.

3. Also, is there any evidence for the ~3-hour separation between L0 and L1? Wright et al. 2022 report what they called primary and secondary Lamb waves (not sure if they match L0/L1), but the time difference is about 60-min. This study ([https://agupubs.onlinelibrary.wiley.com/doi/10.1029/2023 GL103809](https://agupubs.onlinelibrary.wiley.com/doi/10.1029/2023%20GL103809)) presents L1 mode also in the mesosphere. From wind measurements, the Lamb wave L1 mode period

(2-hr), wavelength (1400 km), and wave pattern (a solitary wave) seem not to match what is presented in the airglow. And very interesting, they do not see L0 mode and argue that L0 mode is likely a higher-frequency wave and got averaged out.

Response:

Thank you very much for your comment. This is a good question. We think that the time interval between L0 and L1 is not a constant, but rather anisotropic due to the influence of the background atmosphere. Thank you very much for providing the references Sepúlveda et al. (2023) and Poblet et al. (2023).

According to Figure 1 of Sepúlveda et al. (2023). We can estimate that the time it takes for the L0 to reach South America is approximately 13 UT, on January 15, 2022, while the time it takes for L1 to reach South America is approximately 18 UT (Poblet et al., 2023), with a time interval of approximately 5 hours between the two wave modes.

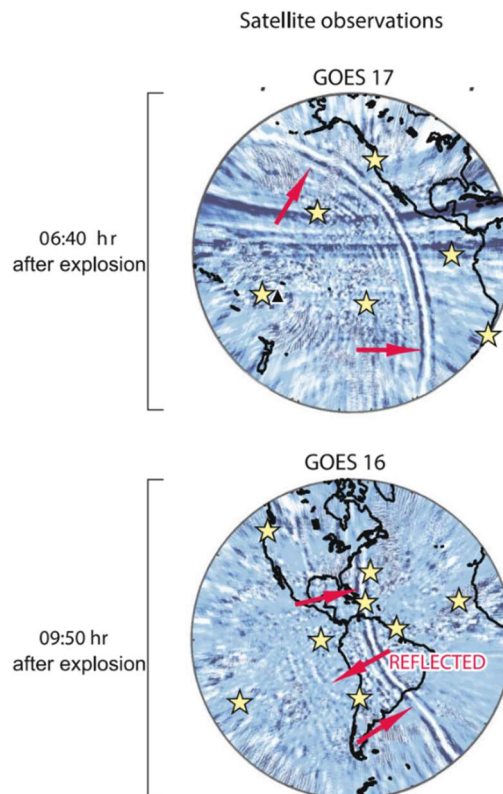


Figure 1 of Sepúlveda et al. (2023)

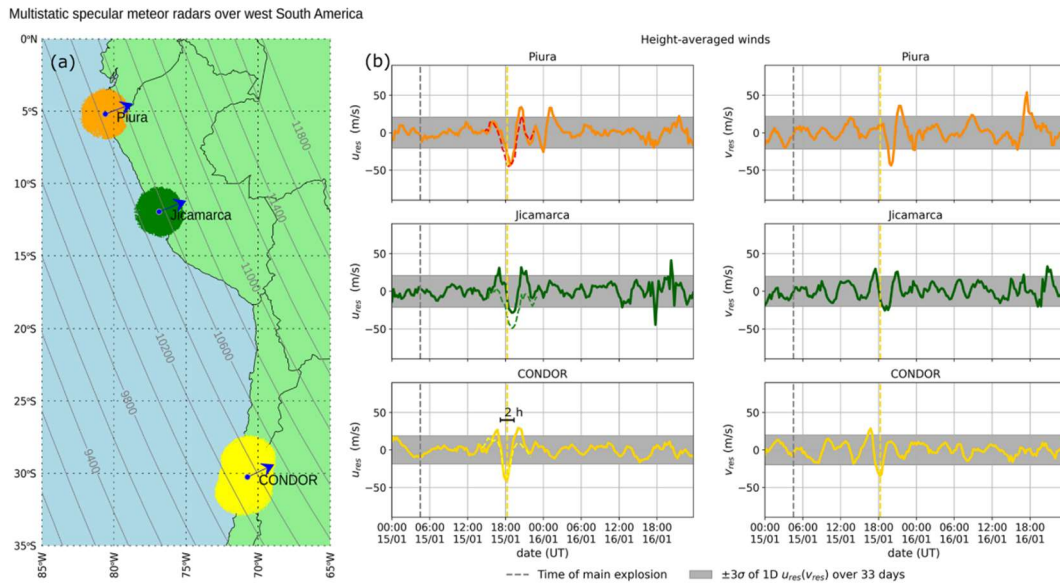


Figure 2 of Poblet et al. (2023)

In the northern hemisphere, over Chinese Mainland, Li et al. (2023) used dense global navigation satellite system data from China to track the propagation of traveling ionospheric disturbances (TIDs) triggered by the 2022 January 15 Tonga volcanic eruption.

They found two group of TIDs corresponding to L0 and L1, respectively. The time for TID related to L0 to reach the Chinese Mainland is about 11:00 UT, while the time for TID related to L1 to reach the Chinese Mainland is about 13:30 UT. The time interval between the two is 2.5 hours, which is very close to the 3-hour interval we observed.

References

- Li, X., Ding, F., Yue, X., Mao, T., Xiong, B., & Song, Q. (2023). Multiwave structure of traveling ionospheric disturbances excited by the Tonga volcanic eruptions observed by a dense GNSS network in China. *Space Weather*, 21, e2022SW003210. <https://doi.org/10.1029/2022SW003210>
- Poblet, F. L., Chau, J. L., Conte, J. F., Vierinen, J., Suclupe, J., Liu, A., & Rodriguez, R. R. (2023). Extreme horizontal wind perturbations in the mesosphere and lower thermosphere over South America associated with the 2022 Hunga eruption. *Geophysical Research Letters*, 50, e2023GL103809. <https://doi.org/10.1029/2023GL103809>
- Sepúlveda, I., Carvajal, M., & Agnew, D. C. (2023). Global winds shape planetary-scale Lamb waves. *Geophysical Research Letters*, 50, e2023GL106097. <https://doi.org/10.1029/2023GL106097>

4. For tsunami-generated gravity waves (#3—#5 in this manuscript), they have been studied in many model simulations. (<https://agupubs.onlinelibrary.wiley.com/doi/full/10.1029/2022JA030301>, <https://agupubs.onlinelibrary.wiley.com/doi/10.1029/2020JA028309>, <https://agupubs.onlinelibrary.wiley.com/doi/full/10.1002/2016JD025673>). However, it seems the ocean surface vertical displacements need to be large enough (10 cm or even higher) to produce 1% airglow fluctuations, Table 3 of Inchin et al. (2022). Otherwise, the wave signature might not be detectable in the mesosphere airglow. This is another reason that you need to carefully estimate the observed wave amplitudes in airglow fluctuation percentage. Another drawback of this part is the tsunami simulations were not verified, such as by DART buoy wave height measurements as well as many published studies.

I am very skeptical about the gravity waves being tsunamis generated if the surface wave height is in the order of 2 cm, as shown in Figure 6. Weak tsunamis likely won't generate atmospheric gravity waves. It might even be the opposite; those weak tsunamis are possibly excited by atmospheric gravity waves. (<https://www.nature.com/articles/s41586-022-04926-4> and <https://www.nature.com/articles/s41598-022-25854-3>). This Figure (<https://www.nature.com/articles/s41586-022-04926-4/figures/6>) demonstrates the observed tsunamis are very well simulated. The order of magnitudes of the tsunami's surface height is somewhat similar to the 2 cm for two sites, 21416 and 23219, both similar distances to the East China Sea from the Tonga volcano.

Response:

Thank you very much for your comment. This is a great question. There have been theoretical (Peltier and Hines, 1976) and observational (Grave and Makela, 2015, 2017) studies on the relationship between the amplitude of tsunamis and gravity waves.

Peltier and Hines (1976) found that a tsunami amplitude of ± 1 cm at sea level can cause vertical motion of ionospheric E layer and F layer ± 100 m. A more direct observational evidence is that Grave and Makela (2017) provided airglow observation of tsunami-generated ionospheric signatures over Hawaii caused by the 16 September 2015 Illapel earthquake. They found that vertical disturbances on the sea surface not exceeding 2 cm (Figure 3b of Grave and Makela (2017)) can create detectable signatures in the ionosphere (Figure 1 of Grave and Makela (2017)).

Therefore, there is no doubt that the generation of gravity waves by this sea surface variation (the order of 2 cm) and their propagation to the middle atmosphere are credible.

The models for the 2022 Hunga Tonga-Hunga Ha'apai Volcanic Eruption used in our study was estimated and validated with observations at offshore DART stations around the Pacific Ocean in a previous study (Figure 3 and Figure 7 of Gusman et al., 2022; <https://link.springer.com/article/10.1007/s00024-022-03154-1>).

On the other hand, we have also demonstrated through ray tracing method that the waves observed in the airglow originate from simulated tsunami waves. So we believe that our tsunami simulation results are reliable.

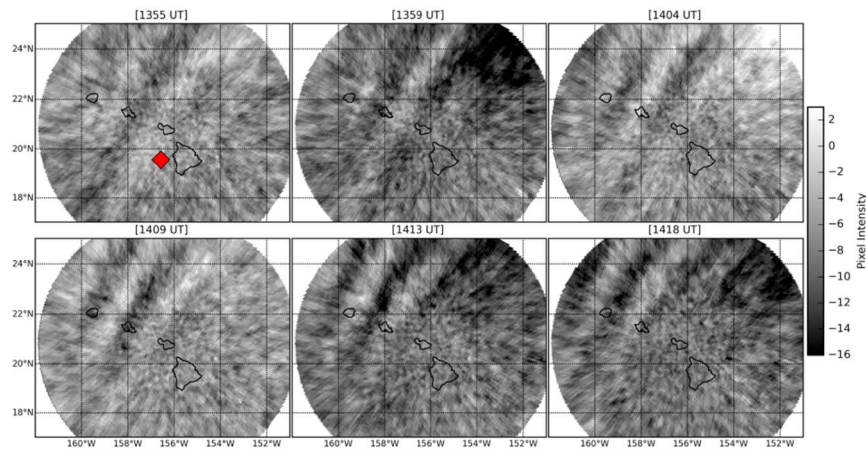


Figure 1. All frames of the filtered 630.0 nm airglow with a visible signature during the arrival of the tsunami to Hawaii on 17 September 2015. The structure is propagating to the northwest. The red diamond in the top left image shows the location of DART station 51407.

Figure 1 of Grawe and Makela (2017)

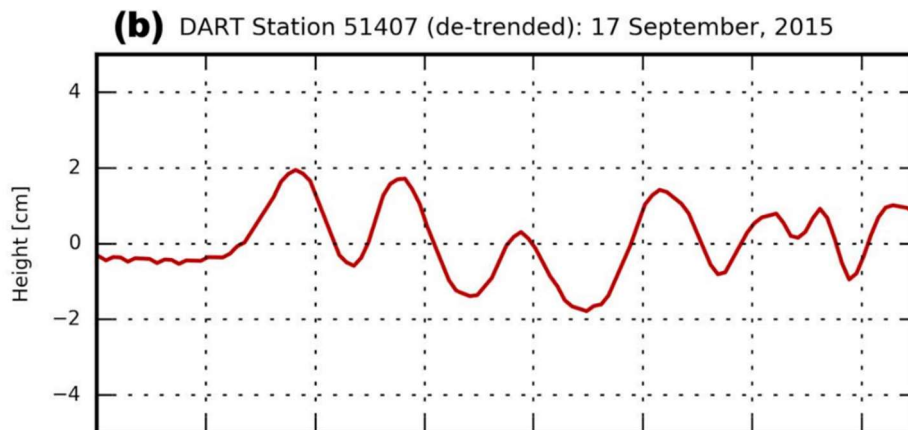


Figure 3b of Grawe and Makela (2017)

References

Grawe, M. A., and J. J. Makela (2015), The ionospheric responses to the 2011 Tohoku, 2012 Haida Gwaii, and 2010 Chile tsunamis: Effects of tsunami orientation and observation geometry, *Earth and Space Science*, 2, 472–483, doi:10.1002/2015EA000132.

Grawe, M. A., and J. J. Makela (2017), Observation of tsunami-generated ionospheric signatures over Hawaii caused by the 16 September 2015 Illapel earthquake, *J. Geophys. Res. Space Physics*, 122, 1128–1136, doi:10.1002/2016JA023228.

Peltier, W. R., and C. O. Hines (1976), On the possible detection of tsunamis by a monitoring of the ionosphere, *J. Geophys. Res.*, 81(12)

5. Many other studies that report the Tonga eruption-related waves did a statistical analysis to verify the observed perturbations on that day were not random or just background (they exist even if there is no volcano eruption). Basically, they take a long-term average of several days to get a background perturbation. In your case, make sure you do not see those similar waves every day. If you observe something different before and after that day, then you can tell what you observe on that day is eruption-related. For the reason above, the selected snapshot-style airglow images at several time steps are not very robust evidence for such volcano/tsunami-related waves. Keograms or movies can better demonstrate the arrival of the waves. Also, you need to add the distance to the volcano on the map.

Response:

Thank you very much for your suggestion. This is a very good question.

According to your suggestion, we have made animations of the day of the Tanga volcanic eruption(<https://doi.org/10.5446/66190>), as well as two days before and after Tanga eruption (<https://av.tib.eu/series/1689>; **Movie S1** corresponds to January 13th, **Movie S2** corresponds to January 14th, **Movie S3** corresponds to January 16th, and **Movie S4** corresponds to January 17th), as supporting materials. Through animation, it can be found that the observation of the airglow is very calm before and after Tanga eruption, while on the day of the eruption, severe disturbances were observed and the wave propagation direction comes from the Tonga direction. Therefore, there is a strong correlation between the atmospheric fluctuations observed on the day of the Tanga eruption and the Tonga volcanic eruption.

At the same time, we have also added the following Figure, including the station name and distance from the Tonga volcano.

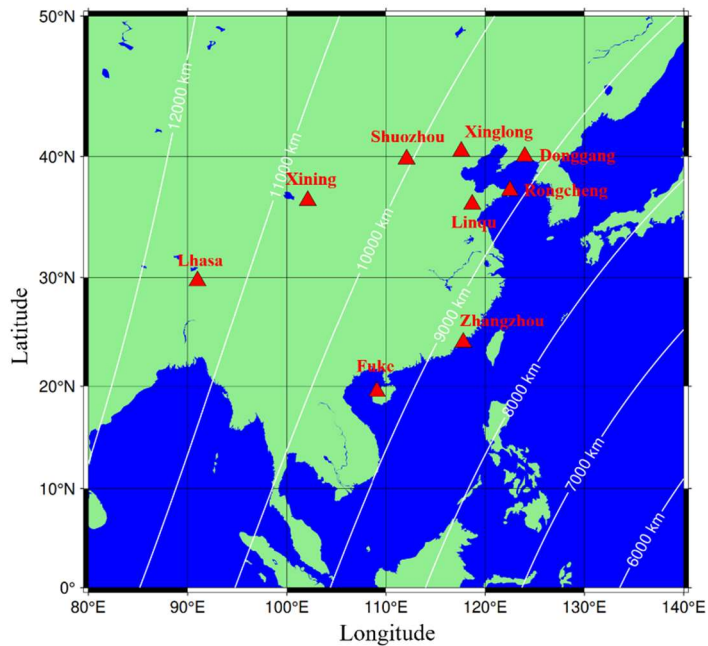


Figure 1 The distribution of airglow network stations, along with the large circular centered on the Tonga volcano and its radius length, is also marked in the figure

Section 3.2, Figures 5 and 6 present results about the tsunami simulation, but not many details are included, are they verified?

Response:

Thank you very much for your comment. This is a very good question.

It is necessary to verify the models through observation results. As mention above, the models for the 2022 Hunga Tonga-Hunga Ha’apai Volcanic Eruption used in our study was estimated and validated with observations at offshore DART stations around the Pacific Ocean in a previous study (Figure 3 and Figure 7 of Gusman et al., 2022; <https://link.springer.com/article/10.1007/s00024-022-03154-1>).

On the other hand, we have also demonstrated through ray tracing method that the waves observed in the airglow originate from simulated tsunami waves in the coastal areas of China. So we believe that our tsunami simulation results are reliable.

All figures and corresponding discussions: Add the lapse time since the volcano eruption in all the figures, which could better help to understand the evolution of the wave pattern.

Response:

This is a very good suggestion. We add the lapse time since the volcano eruption in the figures.

21, airglow imaging system network or airglow imager network.

Response:

“a ground-based airglow network” is changed to “a ground-based airglow imager network”.

22, I anticipate this ‘phase speed’ is horizontal phase speed or total phase speed.

Response:

Yes, you are right. “phase speed” is changed to “horizontal phase speed”.

24, confusing, L0 and L1 wavefront is vertical, then L0 wavefront mode tilts forward.

Response:

The characteristics of the theoretically (Lindzen and Blake, 1972) predicted L0 mode is that the phase lines of the wavefront are vertical up to the lower thermosphere and tilt outward above. As for Lamb wave L1 mode, the ground and mesopause region provide waveguide surfaces, resulting in maximum wave energy between the two layer, while the phase does not change with height (Francis, 1973).

References

Francis, S. H.: Acoustic-gravity modes and large-scale traveling ionospheric disturbances of a realistic, dissipative atmosphere, *J. Geophys. Res.*, 78 (13), 2278– 2301,1973.

Lindzen, R. S., and Blake, D.: Lamb waves in the presence of realistic distributions of temperature and dissipation, *Journal of Geophysical Research*, 77(12), 2166–2176, 1972.

42-44, if you explicitly mention ‘this volcanic eruption,’ I would expect that those waves are all reported from this eruption, so what is the purpose of those old references, even if they are very classic?

Response:

Thank you for your comments. Those old references are removed from the manuscript.

54, GNSS TEC, better to give the full name, at least for TEC.

Response:

Thank you very much for your suggestion.

The full name of GNSS TEC is global navigation satellite system (GNSS)- total electron content (TEC), which is added to the manuscript.

73, conventional tsunami, sounds unclear here.

Response:

Thank you for your comments.

We have defined “conventional tsunami” as follows

Conventional tsunamis are typically generated by localized sea surface displacements caused by sources such as earthquakes and volcanoes, similar to the tsunamis directly induced by the 2022 Tonga volcano eruption (TITVE).

74, only two studies, maybe because they are rare.

Response:

“only two studies” is changed to “only two rare studies”.

83, better use one extra sentence to describe the term in ().

Response:

Thank you very much for your suggestion. “(air-water-air-coupling process)” is changed to “through air-water-air-coupling process”.

90-91, I guess there are two filters used on the same lens; basically, it is the same equipment. It is a little confusing to declare two airglow networks. Also, clearly state what types of airglow are observed.

Response:

Thank you very much for your comments.

In order to achieve higher temporal resolution, they are independent of each other, meaning that one filter corresponds to one lens. So, various types of airglow, including OH, OI 557.0 nm, 630.0 nm, and Na airglow have been observed. But in this study, we mainly used OH and OI 630.0 nm airglow.

105, what is “moving change pressure”

Response:

The moving change pressure is used as input for the momentum equation of tsunami simulation. It changes with distance and time from the center of the Tonga volcanic eruption (Gusman et al., 2022).

References

Gusman, A. R., Roger, J., Noble, C. et al. The 2022 Hunga Tonga-Hunga Ha'apai Volcano Air-Wave Generated Tsunami, Pure and Applied Geophysics, 2022.

107, I would expect to see a brief here about the tsunami simulation and some more details like section 2.3.

Response:

Thank you very much for your comments. We have provided a more detailed description of the tsunami model simulations

2.2 Tsunami simulation model

Tonga submarine volcano erupted on 15 January 2022, and generated tsunamis that were detected around the globe, affected particularly the Pacific region. In this study, two types of tsunamis were simulated, conventional tsunami simulations and atmospheric pressure wave-induced tsunami simulations. The linear-shallow water equations in the spherical coordinate system are used to simulate the tsunamis from the localized source and atmospheric pressure wave. The continuity equation of a linear shallow water wave model in spherical coordinates is:

$$\frac{\partial \eta}{\partial t} + \frac{1}{R \sin \theta} \left[\frac{\partial (ud)}{\partial \varphi} + \sin \theta \frac{\partial (vd)}{\partial \theta} \right] = 0 \quad (1)$$

where η is free surface elevation (m), d is the water depth (m), R is the Earth's radius (6371,000 m), φ is longitude, θ is colatitude.

While the momentum equations of the linear shallow water wave model are:

$$\frac{\partial u}{\partial t} + \frac{1}{R \sin \theta} \left[g \frac{\partial \eta}{\partial \varphi} + \frac{1}{\rho} \frac{\partial p}{\partial \varphi} \right] + fv = 0 \quad (2)$$

$$\frac{\partial v}{\partial t} + \frac{1}{R} \left[g \frac{\partial \eta}{\partial \theta} + \frac{1}{\rho} \frac{\partial p}{\partial \theta} \right] - fu = 0 \quad (3)$$

where, u is the velocity along the lines of longitude (m/s), v is the velocity along

the lines of latitude, g is the gravitational acceleration (9.81 m/s^2), p is the atmospheric pressure (Pa), ρ is the sea water density (1026 kg/m^3), f is the Coriolis coefficient. For the atmospheric pressure wave-induced tsunami simulation, the moving change pressure terms as an input to tsunami simulation momentum equation. The atmospheric pressure wave model is based on the Equation (1) in Gusman et al. (2022).

For the tsunami simulations from a localized source, a B-spline function (Koketsu and Higashi, 1992) below is used to represent the circular water uplift source at the volcano:

$$f(x, y) = \sum_{i=0}^3 \sum_{j=0}^3 c_{k+i, l+j} B_{4-i}\left(\frac{x-x_k}{h}\right) B_{4-j}\left(\frac{y-y_l}{h}\right) \quad (4)$$

where

$$B_i(r) = \begin{cases} r^3/6, & i = 1 \\ (-3r^3 + 3r^2 + 3r + 1)/6, & i = 2 \\ (3r^3 - 6r^2 + 4)/6, & i = 3 \\ (-r^3 + 3r^2 - 3r + 1)/6, & i = 4 \end{cases} \quad (5)$$

x_k and x_l stand for the coordinates of the knots along the x and y axes, h is the characteristic diameter of water uplift, r is the great-circle distance from the volcano eruption center, $c_{1,1} = 1$ and the other $c_{k+i, l+j} = 0$. In this study, the modelling domain covers the Pacific Ocean and some parts of Indian Ocean and the Caribbean with a grid size of 5 arc-min. For detailed tsunami simulation algorithms, please refer to Gusman et al. (2022).

125, is there any detrending or filtering on the SABER temperature before it is used in the calculation?

Response:

The temperature product provided by TIMED/SABER team directly represents the background atmospheric temperature and does not require detrending or filtering processing.

Line 141, do not use the alphabet o for a degree; use the math symbol.

Response:

It has been modified.

Section 3.1 and Figure 1, better give each station a name or a number, so you could clearly state the wave front was visible in which station.

Response:

Thank you very much for your good suggestion.

We have added the following Figure 1, including the station name and distance from the Tonga volcano.

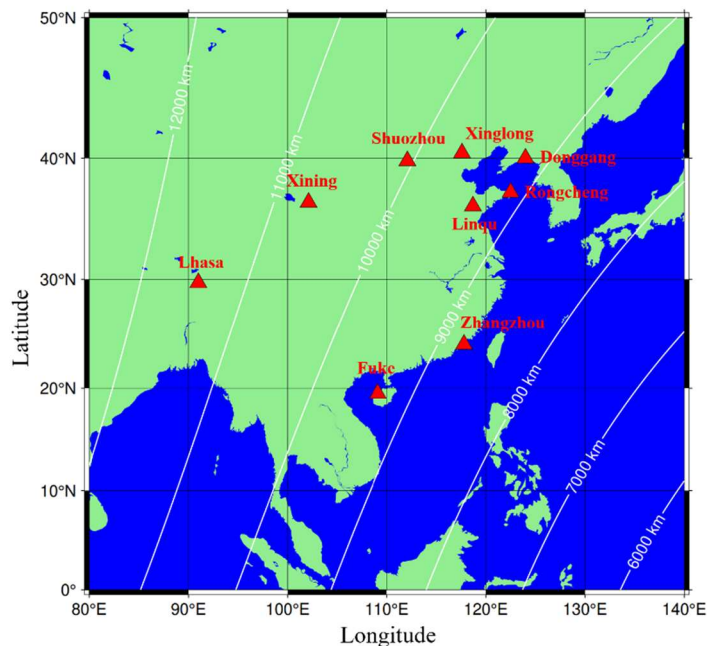


Figure 1 The distribution of airglow network stations, along with the large circular centered on the Tonga volcano and its radius length, is also marked in the figure

Figure 1, in sub-Figure 6 (middle row, right), P1-P6 are labeled; what are they? In sub-Figures 8 and 9, what are early and late wave packets?

Response:

We have made adjustments to Figure 1 (Figure 3 in revised manuscript) and provided explanations for the markings in it.

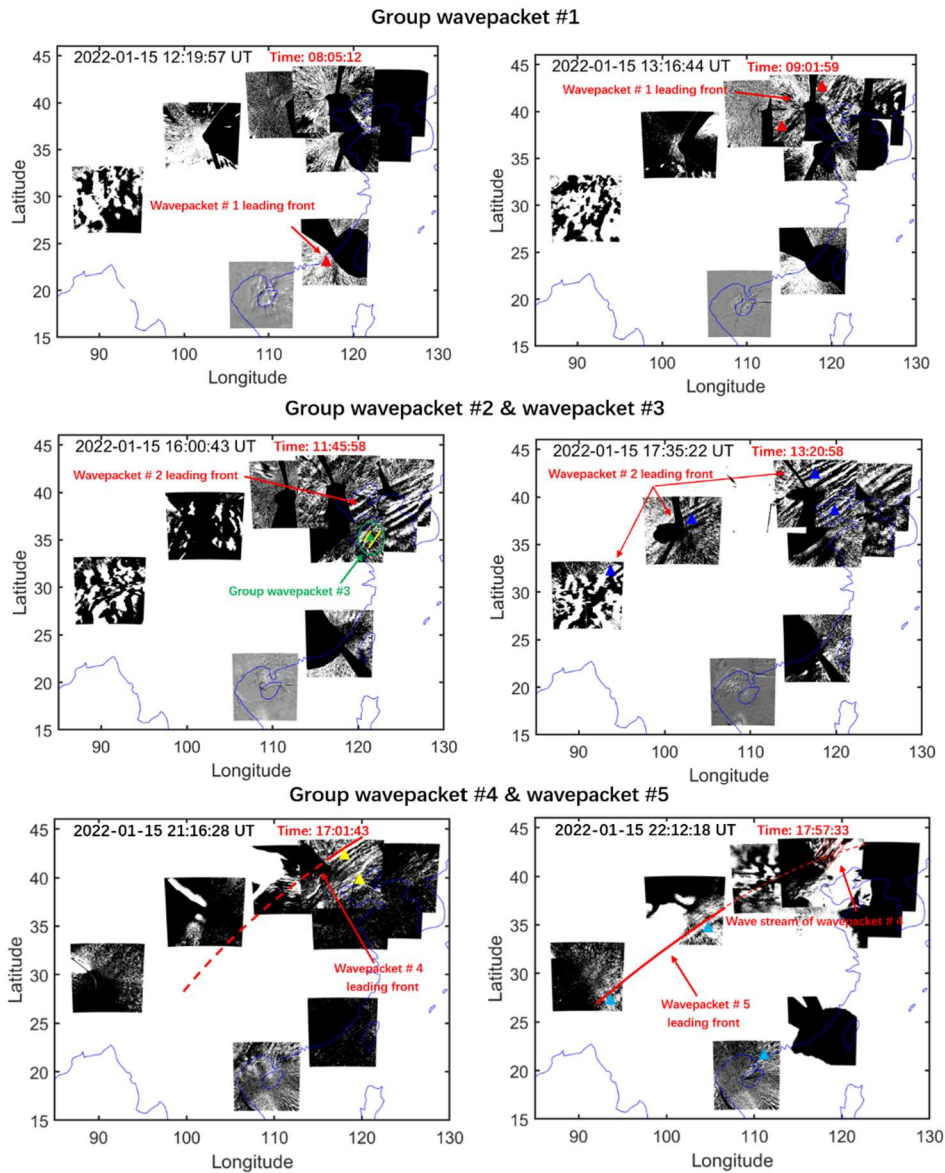


Figure 3 Five strong group atmospheric waves associated with the Tonga volcano eruptions were observed in the mesopause region by the ground-based airglow network. Different colored triangles correspond to each wave event sampling point, while red, blue, green, yellow, and cyan correspond to wave packet #1, #2, #3, #4, and #5, respectively. The red time markers in this figure and the following figure represent the lapse time since the volcano eruption.

Figure 1: the labels are often obscured by the airglow images on the map, hard to read. There are plenty of blank areas between airglow images where you can put those labels.

Response:

Thank you very much for your suggestion.

We have put the labels in blank areas.

Figure 1: what happened in sub-Figure 1-6 (top and middle rows) for the station over the 110E and 20S, on that island?

Response:

Thank you very much for your carefully review.

We have reprocessed the data over the 110E and 20S.

Figure 1: for the station over the 120E, 25S, it seems it does not provide much information due to weather.

Response:

Thank you very much for your comment.

Yes, you are right. This is due to weather conditions. To maintain the completeness of the data, we added them to the Figure.

Figure 1, after I checked all the information on the figure, I went to find if any supplementary materials, such as videos showing the motion of the 5 wave packets, are available. Unfortunately, I did not find any. Can the authors make some videos from the airglow images?

Response:

Thank you for your criticism and comments

According to your suggestion, we have made videos of the day of the Tanga volcanic eruption (<https://doi.org/10.5446/66190>), as well as two days before and after Tanga eruption (<https://av.tib.eu/series/1689>), as supporting materials.

149-155, how are those wave phase speeds and amplitudes estimated? For reference, what is the speed of sound at the same altitudes?

Response:

As mention above, the wave parameters are obtained from cross spectral analysis. As your suggestion, we calculate the speed of sound using the following equation

$$c_s = \sqrt{\gamma RT} \quad \gamma = 1.4 \quad R = 287.06 \text{ J/(kg}\cdot\text{K)}$$

We found that the sound speed at the height of the OH airglow is approximately 294 m/s, slightly lower than the speed of lamb wave L0 mode at this height.

Figure 2: you need to clarify the P1-P6 points, even if you show them in Figure 1. Why only information of wave #1-#3 is shown, not wave #4-#5.

Response:

Thank you very much for your comment.

The original Figure 2 has been replaced by the following figure.

Figure 4 shows the distribution of wave parameters for multi-group of atmospheric waves (wave packet #1-#5). The phase speed of wave packet #1 is approximately 309 m/s. Wave packet #2 displays a slightly slower phase speed, with average phase speed of 236 m/s. The horizontal phase velocity of group wave packet # 3-5 is less than that of the first GW, which is mainly distributed in the range of 200 m/s to 215 m/s. The horizontal wavelengths of these five group wave packets are mainly distributed in 80 km-105 km, while the observation period is relatively small and mainly concentrated in 5.7 min-7.2min. For amplitude, the average amplitude of the lamb wave L1 mode (5.4%) is higher than that of the lamb wave L0 mode (3.2%). Wavepacket # 3, # 4, and # 5 have relatively small amplitudes, mainly distributed between 0.85% and 1.25%.

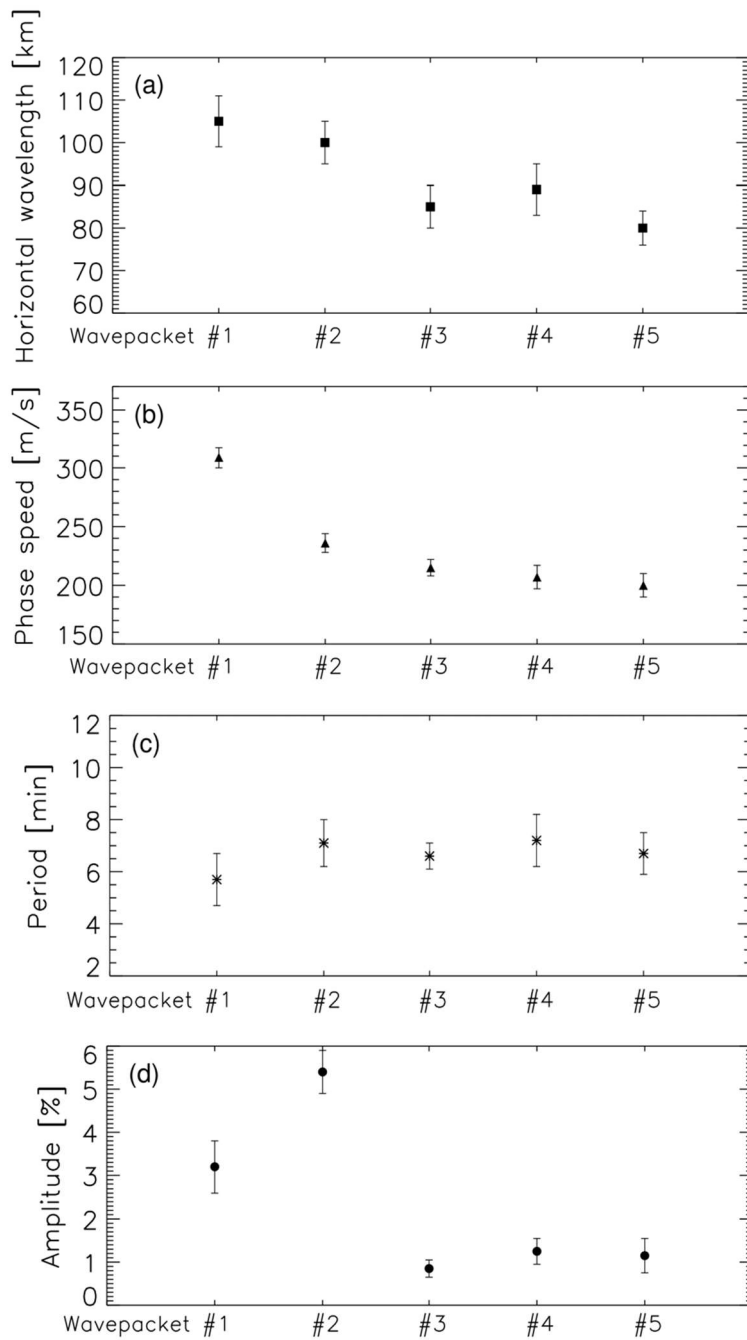


Figure 4 Distribution of (a) wave wavelength, (b) velocity, (c) period, and (d) amplitude parameters for multi-group of atmospheric waves (wave packet #1-#5). The calculation of wave packet parameters comes from the average value of the wave passing through the sampling points in Fig 3.

Figure 2: wave amplitudes in the airglow intensity need a better qualification using the percentage of the airglow intensity fluctuations rather than arbitrary units.

Response:

Thank you very much for your suggestion.

The original Figure 2 has been replaced by the following figure. The amplitude is represented as a percentage instead of the original arbitrary units.

159-161, this statement about vertical distribution is too much for what you showed in Figure 3, where only wave information from three layers is shown, and only Lamb waves.

Response:

Thank you for your comments

The following sentence may cause confusion and has been removed from the revised manuscript.

Figure 3 shows vertical distribution characteristics of atmospheric waves caused by Tonga volcano eruption from the surface to the thermosphere atmosphere.

167, are you able to verify the results by estimating the speed * travel time to be the distance between two sites?

Response:

Thank you very much. This is a very good suggestion.

Figure S1 (below) presents that the time it takes for Lamb L0 mode to reach the zenith direction of Zhangzhou station is approximately 12:19:57 UT, and the time it takes to reach the zenith direction of Xinglong station is approximately 13:13:34 UT, with a time interval of approximately 53.5 min. From Figure 1, it can be seen that the radial distance between the two stations with Tonga volcano as the center is approximately 9700 km. Therefore, we can estimate the velocity of a to be approximately 304 m/s, which is very close to the results obtained from cross spectral analysis.

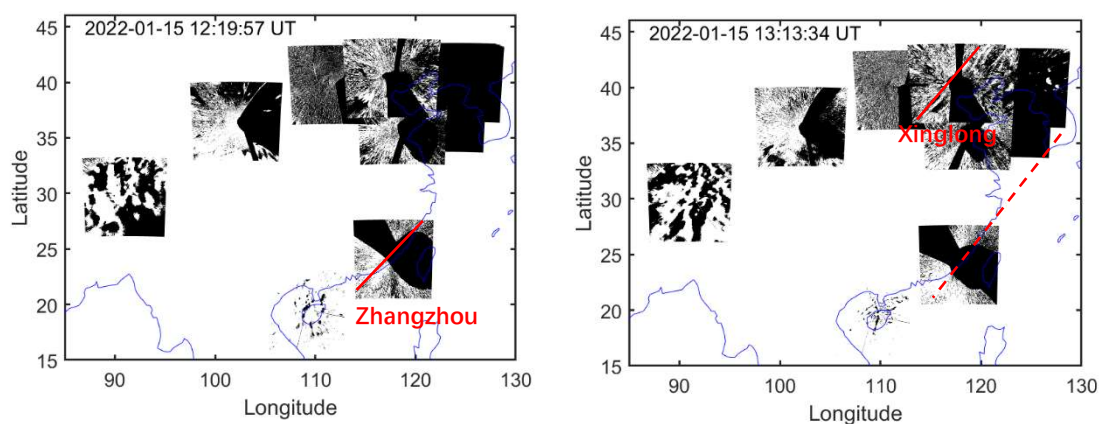


Figure S1

179-185, the scale height between two types of waves only accounts for how fast the wave energy attenuates with respect to altitude; you need wave amplitudes at the source level to compare the observed wave amplitudes at the mesosphere.

Response:

Thank you very much for your good suggestion.

Yes, you are right. We need wave amplitudes at the source level to compare the observed wave amplitudes at the mesosphere.

As your suggestion, we performed derivative processing on the pressure data, as shown by the red line in Fig 5f. We found that the pressure disturbances corresponding to λ_0 and λ_1 are $P1_surface=0.95$ hPa and $P2_surface=0.19$ hPa, respectively. Assuming the scale height $H=8$ km, we estimated the amplification of the two reaching the OH airglow layer with $e^{\kappa z/H}$ and $e^{z/2H}$ as growth rates. $\kappa = (\gamma - 1)/\gamma$, and γ is the ratio of specific heats (~ 1.4). The amplitude of internal waves increases with height at a rate greater than that of Lamb wave L0 mode. Through calculation, we found that $P1_OH = P1_surface * e^{\kappa z/H} = 21.28$ hPa, $P2_OH = P2_surface * e^{z/2H} = 43.83$ hPa.

Although the pressure corresponding to Lamb wave L1 mode on the surface is much lower than that corresponding to L0 mode, at the height of the OH airglow layer, the pressure corresponding to L1 mode is twice that of L0 mode.

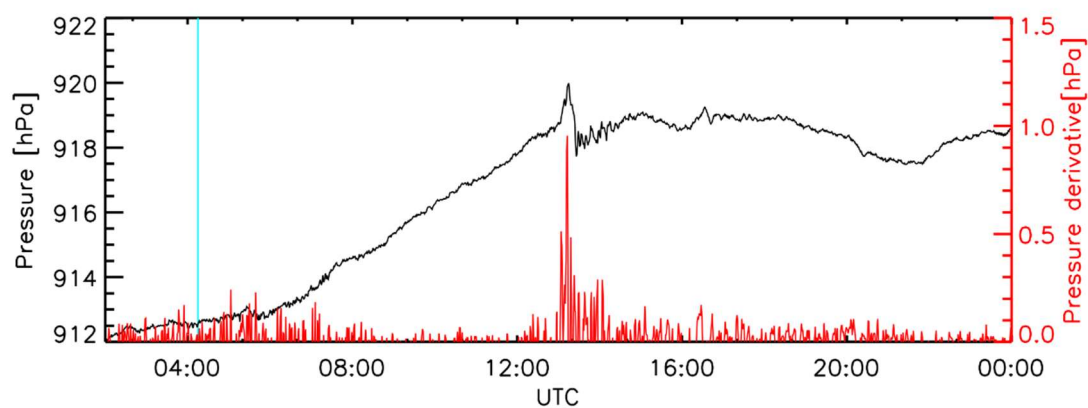


Figure 5f The surface time series of surface pressure obtained from Xinglong observation station. The red line represents the time derivative of the pressure. The sudden change of air pressure at 13:15 UT indicates the arrival time of Lamb wave L0. A small disturbance of air pressure occurs at 16:33 UT indicates the arrival time of Lamb wave L1.

Figure 3: the band in OI airglow image is very similar to the overexposure due to clouds or reflections. Still, I would like to see some supporting evidence, like a Keogram or a video. It is better to use the derivative of the pressure to isolate the waves.

Response:

Thank you for your comments.

We carefully verified the data again and created a continuous image below (Figure S2) and an animation(<https://doi.org/10.5446/66280>). We are confident that it is a wave rather than a cloud.

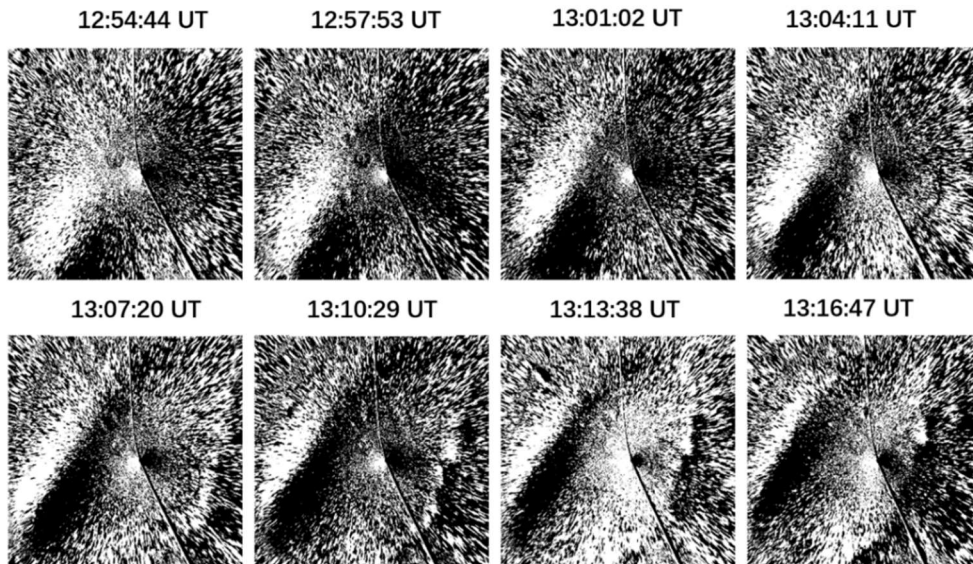


Figure S2

224, many blank spaces are missing; better proofreading is needed.

Response:

Thank you for your comments.

We have carefully checked the entire text to ensure that there are no missing spaces.

Figure 4: yellow lines mark other wavefronts, which is the wave #3.

Response:

I'm sorry we didn't describe clearly. The yellow lines mark the wave #3.

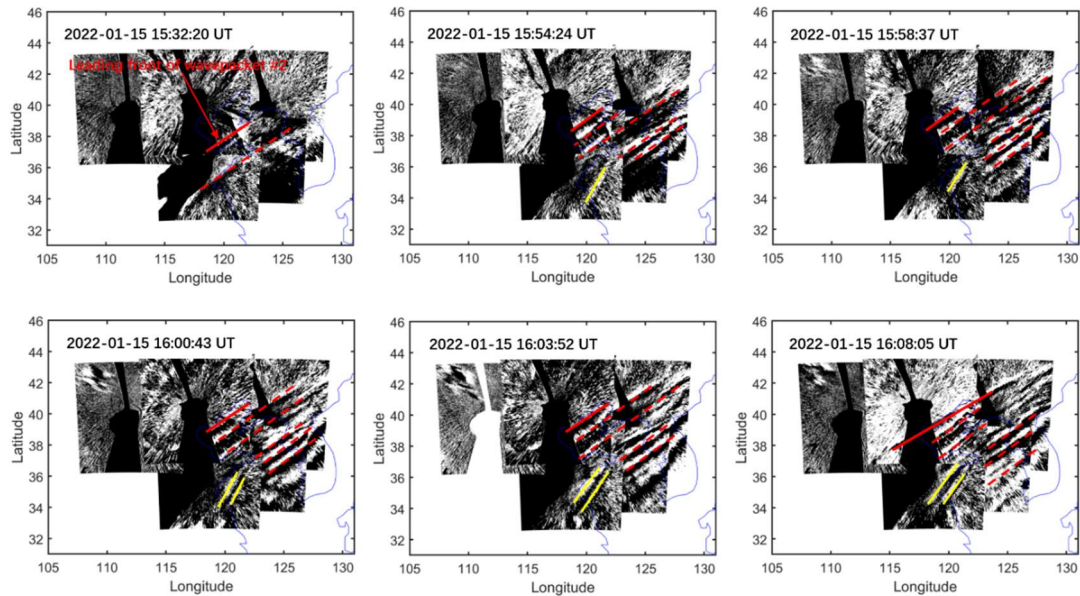


Figure 6 The red solid lines indicate leading wave front of the wave packet #2. The yellow solid lines mark wave packet #3, which are clearly not parallel to the wave fronts of wave packet #2.

Figure 5: up to 5 cm wave height for both types of tsunamis, see comments at the beginning.

Response:

Thank you very much for your comment.

As discussed above, there have been theoretical and observational studies on the relationship between the amplitude of tsunamis and gravity waves. They found that vertical disturbances on the sea surface not exceeding 2 cm can create detectable signatures in the ionosphere. The amplitude of vertical sea level motion in our tsunami simulation is an order of 2 cm (In order to highlight the sea wave, we have limited the display scale to ± 2 cm, the actual amplitude is greater than 2 cm). Therefore, there is no doubt that the generation of gravity waves by this sea surface variation and their propagation to the middle atmosphere are credible.

In terms of models validation, the models for the 2022 Hunga Tonga-Hunga Ha'apai Volcanic Eruption used in our study was estimated and validated with observations at offshore DART stations around the Pacific Ocean in a previous study (Figure 3 and Figure 7 of Gusman et al., 2022; <https://link.springer.com/article/10.1007/s00024-022-03154-1>).

249, how do you calculate the m^2 , which formula was used?

Response:

The calculation of the m^2 is from the Equation below:

$$m^2 = \frac{\omega^2}{c_s^2} \left(1 - \frac{\omega_a^2}{\omega^2}\right) - k^2 \left(1 - \frac{\omega_b^2}{\omega^2}\right)$$

where k is the horizontal wave number from airglow observation, c_s the local speed of sound, $\omega = k(c-u)$ is intrinsic frequency, c is the horizontal phase speed, u is the background wind speed in the direction of wave propagation from meteor radar observations and ERA-5. $\omega_a^2 = \frac{g}{T} \frac{dT}{dz} + \frac{\gamma g}{4H}$ is acoustic cutoff frequency,

$\omega_b^2 = \frac{g}{T} \frac{dT}{dz} + \frac{(\gamma-1)g}{\gamma H}$ is buoyancy frequency, g is the gravitational acceleration, and T

is temperature from the Sounding of the Atmosphere using Broad band Emission Radiometry (SABER) instrument on the Thermosphere Ionosphere Mesosphere Energetics and Dynamics (TIMED) satellite.

The following References that you recommended has been added to the manuscript.

Inchin, P. A., Heale, C. J., Snively, J. B., and Zettergren, M. D.: The dynamics of nonlinear atmospheric acoustic-gravity waves generated by tsunamis over realistic bathymetry, *Journal of Geophysical Research: Space Physics*, 125, 2020.

Inchin, P. A., Heale, C. J., Snively, J. B., and Zettergren, M.D.: Numerical modeling of tsunami-generated acoustic-gravity waves in mesopause airglow, *Journal of Geophysical Research: Space Physics*, 127, 2022.

Laughman, B., D. C. Fritts, and T. S. Lund (2017), Tsunami-driven gravity waves in the presence of vertically varying background and tidal wind structures, *J. Geophys. Res. Atmos.*, 122, 5076-5096, doi:10.1002/2016JD025673.

Nishikawa, Y., Yamamoto, My., Nakajima, K. et al. Observation and simulation of atmospheric gravity waves exciting subsequent tsunami along the coastline of Japan after Tonga explosion event. *Sci Rep* 12, 22354, 2022. <https://doi.org/10.1038/s41598-022-25854-3>

Omira, R., Ramalho, R.S., Kim, J. et al. Global Tonga tsunami explained by a fast-moving atmospheric source, *Nature* 609, 734–740, 2022. <https://doi.org/10.1038/s41586-022-04926-4>

Otsuka, S. (2022). Visualizing Lamb waves from a volcanic eruption using meteorological satellite Himawari-8. *Geophysical Research Letters*, 49, e2022GL098324. <https://doi.org/10.1029/2022GL098324>

Poblet, F. L., Chau, J. L., Conte, J. F., Vierinen, J., Suclupe, J., Liu, A., & Rodriguez, R. R. (2023). Extreme horizontal wind perturbations in the mesosphere and lower thermosphere over South America associated with the 2022 Hunga eruption. *Geophysical Research Letters*, 50, e2023GL103809. <https://doi.org/10.1029/2023GL103809>

Sepúlveda, I., Carvajal, M., & Agnew, D. C. (2023). Global winds shape planetary-scale Lamb waves. *Geophysical Research Letters*, 50, e2023GL106097. <https://doi.org/10.1029/2023GL106097>

Wright, C. J., et al. Surface-to-space atmospheric waves from Hunga Tonga-Hunga Ha'apai eruption, *Nature*, 609 (7928), 741 – 746, 2022.